PROGRESS IN PHOTOVOLTAICS: RESEARCH AND APPLICATIONS
Prog. Photovolt: Res. Appl. 2012; **20**:21–30
Published online 11 March 2010 in Wiley Online Library (wileyonlinelibrary.com). DOI: 10.1002/pip.942

RESEARCH ARTICLE

Comparison of emitter saturation current densities determined by injection-dependent lifetime spectroscopy in high and low injection regimes

C. Reichel*, F. Granek, J. Benick, O. Schultz-Wittmann† and S. W. Glunz

Fraunhofer Institute for Solar Energy Systems, Heidenhofstrasse 2, 79110 Freiburg, Germany

ABSTRACT

The determination of the emitter saturation current density J_{0e} of symmetrical test structures, analyzed by injection-dependent lifetime spectroscopy (IDLS), in high as well as in low injection regimes is compared. A detailed investigation of the influence of different models for the Auger recombination on the evaluation of the measured minority carrier lifetime is performed. It can be concluded that a good agreement for the extraction of J_{0e} under high and low injection conditions for lightly and highly doped emitters on textured and untextured surfaces was obtained if the Auger parameterization of Kerr *et al.* is applied. For deep-diffused emitter profiles on textured surfaces a significant increase of J_{0e} well above the geometrical surface area ratio of untextured and textured surfaces of 1.7 was observed. A verification of the experimentally determined values for J_{0e} is performed by numerical device simulations. The simulated surface recombination velocity for the investigated emitter doping profiles is in good agreement to analytical calculations. Copyright © 2010 John Wiley & Sons, Ltd.

KEYWORDS

emitter saturation current density; surface recombination velocity; injection-dependent lifetime spectroscopy; quasi-steady-state photoconductance; numerical simulations

***Correspondence**

C. Reichel, Fraunhofer Institute for Solar Energy Systems, Heidenhofstrasse 2, 79110 Freiburg, Germany.
E-mail: christian.reichel@ise.fraunhofer.de

Received 31 March 2009; Revised 8 September 2009

1. INTRODUCTION

Knowledge of the saturation current density of lightly and relatively highly doped emitters J_{0e} is essential for the design and optimization of high efficiency silicon solar cells. In order to reach high efficiencies, a selective emitter is normally applied, consisting of a local highly doped emitter underneath the front grid fingers to reduce the recombination in the contact area as well as the contact resistance, and a lightly doped shallow emitter in between in order to reduce the overall emitter recombination and to achieve a good surface passivation quality. Several investigations for highly and lightly doped phosphorus and boron diffused emitters have been carried out for different doping profiles and passivation layers to reduce the minority carrier recombination at the surface [1–8].

The determination of J_{0e} can be accomplished by means of the injection-dependent lifetime spectroscopy (IDLS). The measurement of the minority carrier lifetime of diffused silicon wafers has been carried out by the quasi-steady-state photoconductance technique (QSSPC) in the quasi-steady-state illumination mode [9]. Currently, this method is widely used in case of lightly doped silicon substrates to extract J_{0e} from the bulk recombination of symmetrical test structures (see Figure 1) [10]. The only assumption which has to be made is a suitable parameterization of the Auger recombination in high injection regimes. When using highly doped silicon substrates, the determination of J_{0e} strongly depends on the bulk recombination [11,12]. Nevertheless, assuming that for high carrier lifetime material the Shockley–Read–Hall recombination can be neglected, it is possible to express the bulk recombination in terms of Auger recombination.

The focus of this study is to compare the extraction of J_{0e} from the bulk recombination under high and low injection conditions and to show the impact of different models for the Auger recombination [13–16] on J_{0e}. Alternatively, the determination of J_{0e} for the investigated emitter profiles by numerical device simulations based on the measured effective minority carrier lifetime curves is

†Now with TetraSun Inc., California, USA.

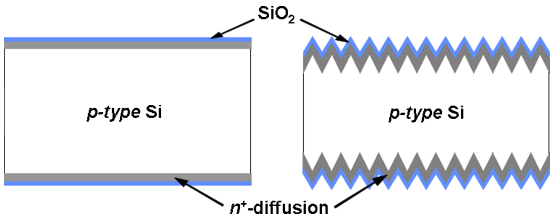

Figure 1. Schematic illustration of the investigated symmetrical test structures for injection-dependent lifetime spectroscopy and the determination of the saturation current density of the diffused emitters.

introduced and compared to the experimental determination of J_{0e} at high and low injections. The correlation between J_{0e} and the phosphorus doping concentration at the surface is shown for samples with textured and untextured surfaces. Based on analytical calculations and numerical device simulations, the corresponding surface recombination velocities S_0 are compared.

2. SAMPLE PREPARATION AND EXPERIMENTAL PROCEDURE

The silicon substrates used within the scope of this investigation have been prepared by Glunz *et al.* [4] The wafers are boron-doped and float-zone grown with a <100> surface crystal orientation. The substrates have a specific base resistivity ρ_{base} of about 0.5 Ω cm and 100 Ω cm for the investigations in low and high injection regimes, respectively, and are 250 μm thick. After RCA cleaning, the phosphorus diffusions were carried out in a tube furnace with a $POCl_3$ liquid source for a duration of 30 min. The diffusion temperatures T were varied from 810°C to 870°C. After the emitter diffusion, a drive-in step for 30 min at the same temperature in an argon atmosphere was applied. For the surface passivation, the phosphorus silicate glass was removed and a dry oxidation at a temperature of 1050°C for 25–40 min was carried out, resulting in an oxide thickness of around 105 nm. This was followed by a post-oxidation anneal at 1050°C for 20 or 120 min in an argon atmosphere. The same process sequences were also applied for samples with textured surfaces (inverted pyramids). The inverted pyramids were prepared by structuring a thermally grown silicon oxide with photolithography and subsequently etching the silicon in a KOH etching solution. The samples finally received a low temperature hydrogenation treatment at 425°C for 25 min in a forming gas ambient, consisting of 5% H_2 + 95% N_2.

The profiles of the diffusions were Gaussian-like and the emitter sheet resistances were in the range of 16 Ω/□ to 290 Ω/□. The diffusion profiles were determined by the stripping-Hall method on untextured surfaces, shown in Figure 2, and the emitter sheet resistances R_{sheet} of the diffused emitters were measured on untextured surfaces by the four-point probe technique. The depths of the *p-n* junctions were relatively deep due to the high-temperature

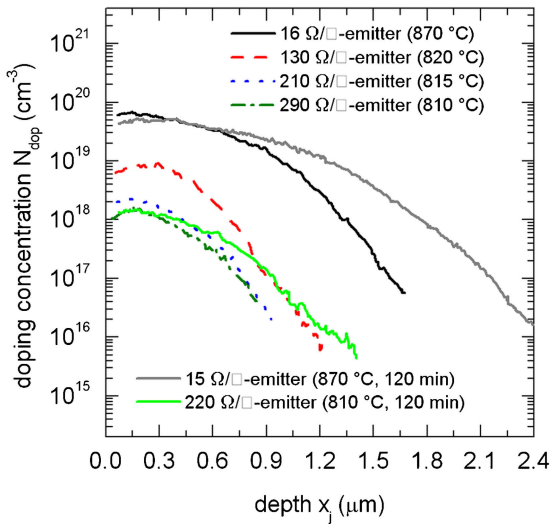

Figure 2. Doping profiles and corresponding emitter sheet resistances for the diffused phosphorus emitters. The diffusion temperatures are shown in brackets and, unless otherwise noted, are for post-oxidation anneal times of 20 min.

post-oxidation anneal and are in the range of 1.0–1.8 μm. Post-oxidation anneal times of 120 min are resulting in profiles with very low phosphorus doping concentrations at the surface and even deeper *p-n* junctions. For example, the emitter with a sheet resistances of 220 Ω/□ is nearly 1.5 μm deep compared to the emitter created at the same diffusion temperature but with a post-oxidation anneal of only 20 min.

3. METHODS FOR THE DETERMINATION OF THE EMITTER SATURATION CURRENT DENSITY UNDER HIGH AND LOW INJECTION CONDITIONS

3.1. High injection regimes

In high injection regimes, where $\Delta n >> N_{dop}$, the recombination in the emitter region can be distinguished from the bulk recombination due to the injection level dependence of the minority carrier lifetime in the emitter region and of the bulk. The extraction of J_{0e} can be performed by taking into account that the Auger recombination is nonlinearly dependent on the excess carrier density, illustrated in Figure 3, whereas the emitter recombination increases linearly with the excess carrier density [12]. At high-level injections, the radiative recombination and the Shockley–Read–Hall recombination in the bulk play no significant role when high minority carrier lifetime material is used. In this case, the bulk minority carrier lifetime is dominated by the Auger recombination whereas the emitter region is still in low injection regimes due to the high doping concentrations.

By plotting the inverse effective minority carrier lifetime reduced by the inverse Auger carrier lifetime

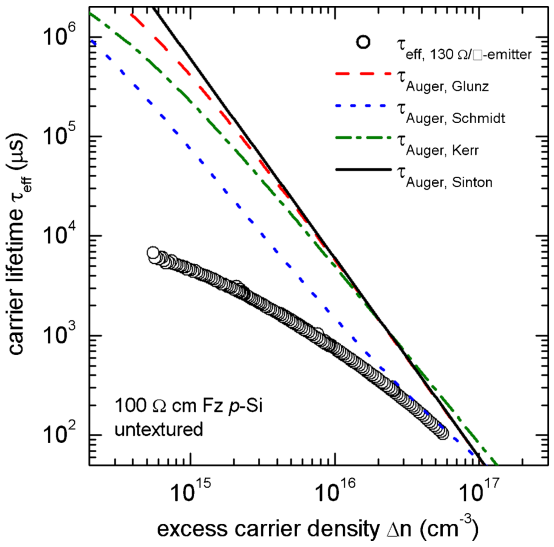

Figure 3. Measured effective carrier lifetime (circles) versus excess carrier density for a *p*-type float-zone silicon sample with a substrate resistivity of 100 Ω cm ($N_{dop} = 1{\cdot}34 \times 10^{14}$ cm^{-3}). Also shown are the carrier lifetimes for the different models of the Auger recombination. At high injections, the model of Glunz *et al.* equals the model of Sinton *et al.*

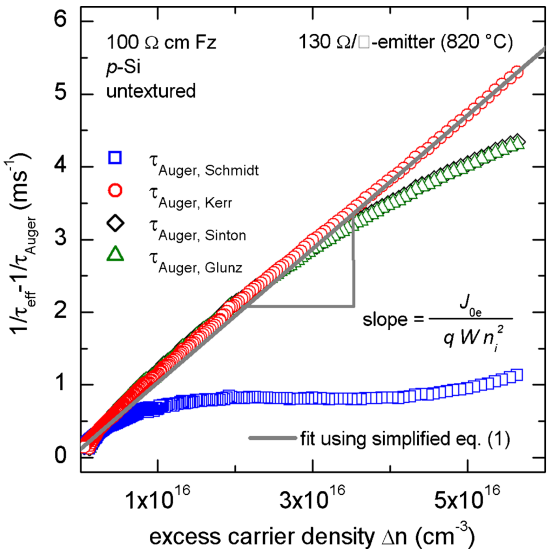

Figure 4. Inverse effective carrier lifetime reduced by inverse Auger carrier lifetime versus excess carrier density for different parameterizations of the Auger recombination. In high injection regimes the model of Glunz *et al.* and Sinton *et al.* are equal.

versus the excess carrier density, it is possible to extract J_{0e}, which is directly proportional to the slope of the resulting curve [10]. The corresponding equation is

$$\frac{1}{\tau_{\text{eff}}} - \frac{1}{\tau_{\text{Auger}}} = \frac{1}{\tau_{\text{SRH}}} + \frac{2J_{0e}}{qn_i^2 W}\left(N_{\text{dop}} + \Delta n\right) \qquad (1)$$

where at high-level injections the term in brackets simplifies to Δn. The only assumption which has to be made for determining J_{0e} is a suitable parameterization of the Auger recombination in high injection regimes with theoretical models, such as presented by Kerr *et al.* [13], Schmidt *et al.* [14], Glunz *et al.* [15], and Sinton *et al.* [16][‡].

The resulting curves of the Auger-corrected effective carrier lifetime versus the excess carrier density of the different models for the Auger recombination are shown in Figure 4 for an untextured sample with an emitter sheet resistance of 130 Ω/□. For a defined range of excess carrier densities between $\Delta n_1 = 3 \times 10^{15}$ cm^{-3} and $\Delta n_2 = 5 \times 10^{16}$ cm^{-3}, fulfilling the requirement of high injection regimes, the slope of the straight lines result in different values for J_{0e}. This is due to the applied models for the Auger recombination. The variation of the excess carrier density range also affects the accuracy of the linear fit of the curves. The determined values for J_{0e} are in the range of 4–7 fA/cm^2 for the model of Schmidt *et al.*, and 13–16 fA/cm^2 for the model of Glunz *et al.* as well as for the model of Sinton *et al.* and 16 fA/cm^2 for the model Kerr *et al.*

With the model of Kerr *et al.*, Glunz *et al.*, and Sinton *et al.*, the extraction of J_{0e} can be performed when the excess carrier density is one order of magnitude higher than the substrate doping concentration. In this case nearly the same values for J_{0e} are determined for the different models. Additionally, the model of Kerr *et al.* can be applied at much higher injection levels due to the linearity over a wide range of excess carrier densities. With the model of Schmidt *et al.*, a nonlinear behavior over a wide range can be observed. In this case, an accurate fit is nearly impossible. However, this behavior is not observed for samples with a highly doped emitter. For lowly doped emitters, much lower values for J_{0e} are determined with the model of Schmidt *et al.* than with the model of Kerr *et al.*, Glunz *et al.*, and Sinton *et al.* In this study, the Auger parameterization of Kerr *et al.* is applied as a wide range of excess carrier densities can be used to extract J_{0e} accurately.

It is worth mentioning that the carrier lifetime measurements were performed at a temperature of 30°C. However, the measured quantity J_{0e}/qn_i^2 has no temperature dependence [§]. Therefore, the results can be reported at a temperature of 25°C corresponding to the intrinsic carrier concentration n_i of 8.79×10^9 cm^{-3} (neglecting the doping dependence due to bandgap narrowing) which has been calculated as proposed by Green [17]. This is in contrast to former reported values of n_i used for the determination of J_{0e} by our group [18,19].

3.2. Low injection regimes

In low injection regimes, where $\Delta n << N_{\text{dop}}$, the recombination in the emitter region cannot be distinguished from

[‡]At high injections only using the Coulomb-enhanced Auger recombination coefficient C_A of 1.66×10^{-30} cm^6/s.

[§]Sinton RA (private communication).

the bulk recombination. However, for a sample without a diffused emitter and a negligible surface recombination, the measured minority carrier lifetime would be limited by the intrinsic bulk minority carrier lifetime $\tau_{bulk,intr}$ which is given by the radiative recombination and the Auger recombination. In silicon, the radiative recombination under low injection conditions plays no significant role. Furthermore, it is assumed that for high minority carrier lifetime material, such as float-zone grown material, the Shockley–Read–Hall recombination does not affect the bulk recombination significantly. In this case, one can assume that the bulk recombination at low injections is solely limited by the Auger recombination. This assumption leads to an upper bound for the determination of J_{0e}. For the more general case of low minority carrier lifetime material, the Shockley–Read–Hall recombination cannot be neglected. In this case, the extraction of J_{0e} will have a large uncertainty and the determined values have to be verified with values of J_{0e} determined at high-level injections. Nevertheless, at low-level injections, equation (1) can be simplified by considering the term in brackets only to be dependent on N_{dop}. It can be applied for lowly injected substrates where the bulk minority carrier lifetime determined by Auger recombination does not depend on the excess carrier density such as in high-level injection, see Figure 5.

The intrinsic bulk minority carrier lifetime $\tau_{bulk,intr}$ of the investigated substrates can be calculated by the different models for the Auger recombination. The determined values for $\tau_{bulk,intr}$ at $\Delta n = 3 \times 10^{15}\,cm^{-3}$ are 493 µs for the model of Schmidt *et al.*, 562 µs for the model of Glunz *et al.* and 706 µs for the model of Kerr *et al.* Additionally, the bulk minority carrier lifetime has been measured at bare silicon wafers immersed in hydrofluoric acid to suppress surface recombination. The bulk minority carrier lifetime was determined to be around 550 µs for undiffused, non-gettered substrates with a resistivity of 0.5 Ω cm. With the model of Glunz *et al.*, and Schmidt *et al.*, an intrinsic bulk minority carrier lifetime in the range of the measured value for $\tau_{bulk,intr}$ has been calculated. The values for $\tau_{bulk,intr}$ with the Auger parameterization of Kerr *et al.* is much higher, thus giving an upper bound for $\tau_{bulk,intr}$. Taking also the measured bulk minority carrier lifetime of 550 µs into account an error margin can be given for the determination of J_{0e} in low injection regime.

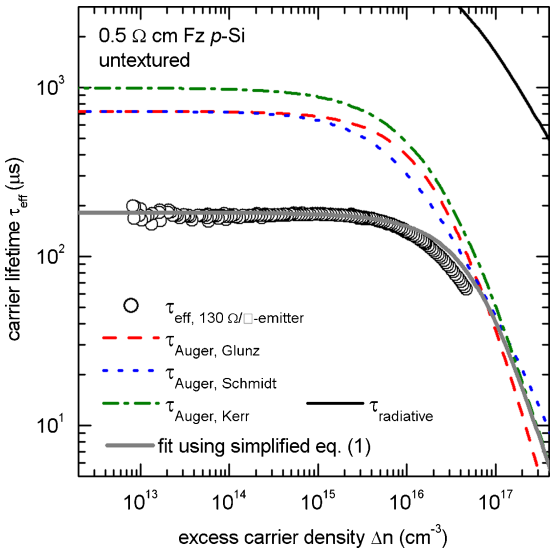

Figure 5. Measured effective carrier lifetime (circles) versus excess carrier density for a *p*-type float-zone silicon sample with a substrate resistivity of 0·5 Ω cm ($N_{dop} = 3{\cdot}26 \times 10^{16}\,cm^{-3}$). Also shown are the carrier lifetimes for the radiative recombination and for the different models of the Auger recombination.

The requirement for low injection is fulfilled for excess carrier densities below $\Delta n = 3 \times 10^{15}\,cm^{-3}$, as shown in Figure 5 for an untextured sample with an emitter sheet resistance of 130 Ω/□. The different parameterizations of the Auger recombination and the nonlinear dependence of the Auger recombination even at quite low-level injections have a direct influence on J_{0e}, calculated by the modified equation (1). With the model for the Auger recombination of Kerr *et al.*, the emitter saturation current density varies from 18 fA/cm^2 to 14 fA/cm^2 for an excess carrier density range of $\Delta n = 5 \times 10^{14}$ and $\Delta n = 3 \times 10^{15}\,cm^{-3}$. The models of Glunz *et al.* and Schmidt *at al.* lead to lower values for J_{0e} and are between 16 and 13 fA/cm^2 and 15 and 12 fA/cm^2, respectively. At low-level injections, the results determined with the model of Schmidt *et al.* and Glunz *et al.* are in good agreement. The model for the Auger recombination of Kerr *et al.* is used in this investigation due to similar reasons as in high injection regimes. The determined values for J_{0e} are slightly higher compared to the other models. Thus, a more conservative estimation is given.

4. APPLICATION OF THE METHODS IN HIGH AND LOW INJECTION REGIMES FOR DIFFERENT EMITTER PROFILES AND SURFACES

4.1. Comparison of the emitter saturation current density determined in high and low injection regimes

The determination of J_{0e} for different emitter profiles with the presented methods in high and low injection regimes for textured and untextured surfaces is shown in Figure 6 and Figure 7. In high injection regimes, different slopes for different emitter profiles can be observed. The extraction of J_{0e} has been performed for excess carrier densities between $\Delta n_1 = 8 \times 10^{15}$ and $\Delta n_2 = 3 \times 10^{16}\,cm^{-3}$, fulfilling the requirement of high-level injection. The linearity of the Auger-corrected minority carrier lifetime curves show that the Auger parameterization of Kerr *et al.* is appropriate for the extraction of J_{0e}. The slope for highly doped emitters is higher than for lightly doped emitters and the slopes of

DOI: 10.1002/pip

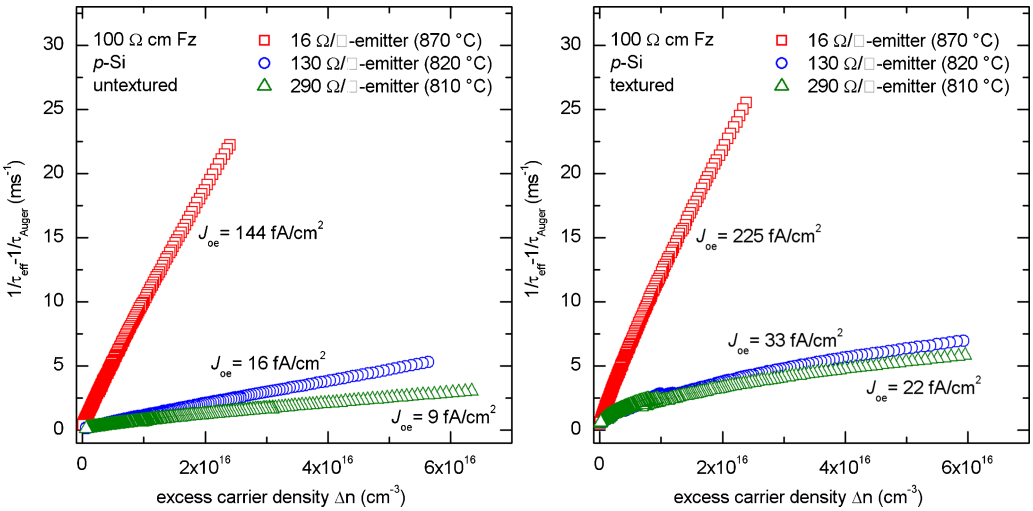

Figure 6. Inverse effective lifetime reduced by inverse Auger lifetime versus excess carrier density for untextured (left) und textured (right) samples with different emitter profiles on *p*-type float-zone silicon with a substrate resistivity of 100 Ω cm.

samples with textured surfaces are higher than for samples with untextured surfaces. The latter observation can be explained with an increase of the surface area due to the inverted pyramids geometry, whereas the former is due to an increase of the Auger recombination in the highly doped emitter region.

For the same reason, the effective minority carrier lifetime curves for samples with highly doped emitters are below the curves of lightly doped emitters and samples with textured surfaces have a lower effective carrier lifetime than samples with untextured surfaces. A comparison of the emitter saturation current density extracted by IDLS in high and low injection regimes, reveals a good agreement for the investigated emitter diffusion profiles. These results show that an accurate determination of J_{0e} can be performed either for lightly or highly doped substrates.

With the information of the emitter saturation current density, it is furthermore possible to calculate the theoretical maximum open-circuit voltage $V_{oc,max}$ via the one diode equation for a symmetrical test structure by

$$V_{oc,max} = \frac{kT}{q} \ln\left(\frac{J_{sc}}{2J_{0e}} + 1\right) \quad (2)$$

whereas a short-circuit current density J_{sc} for the AM1.5G spectrum at an illumination intensity of 100 mW/cm^2 of 38 mA/cm^2 and a temperature of 25°C has been assumed.

In Figure 8 the emitter saturation current density and the calculated maximum open-circuit voltage versus the phosphorus doping concentration $N_{P,0}$ at the surface of test structures with different substrate resistivities for untextured and textured surfaces is shown. Both high and low injection methods for the determination of the emitter saturation current density are in good agreement, see

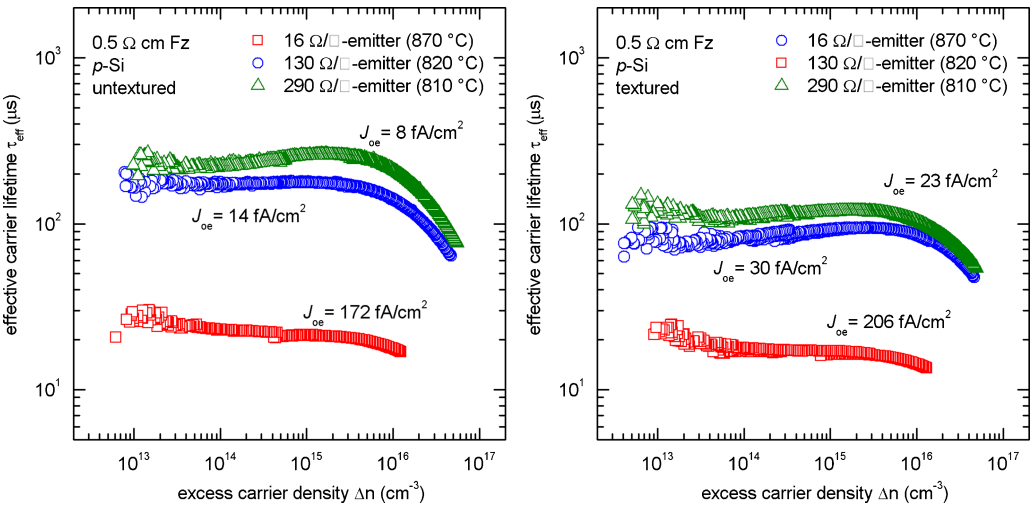

Figure 7. Effective carrier lifetime versus excess carrier density for untextured (left) und textured (right) samples with different emitter profiles on *p*-type float-zone silicon with a substrate resistivity of 0·5 Ω cm. The values for J_{0e} were determined at $n = 3 \times 10^{15}$ cm^{-3}.

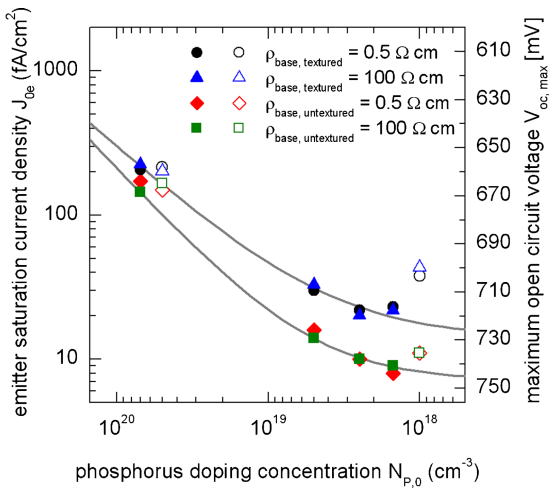

Figure 8. Emitter saturation current density versus phosphorus doping concentration at the surface of symmetrical test structures with different substrate resistivities for untextured and textured surfaces (full symbols). The samples with a post-oxidation anneal time of 120 min are marked (open symbols). The data for the substrate resistivity of 100 Ω cm and a post-oxidation anneal for 20 min have been fitted empirically by the function $J_{0e} = (a\ N_{P,0}{}^b + c)$ A/cm^2. For untextured and textured surfaces, the fitting parameters are $a = 3.728 \times 10^{-36} \pm 4.832 \times 10^{-36}$, $b = 1.137 \pm 0.025$, $c = 7.12 \times 10^{-15} \pm 4.12 \times 10^{-16}$ and $a = 4.388 \times 10^{-32} \pm 8.477 \times 10^{-32}$, $b = 0.941 \pm 0.166$, $c = 1.41 \times 10^{-14} \pm 7.44 \times 10^{-15}$, respectively.

Table I. A decrease of J_{0e} for decreasing $N_{P,0}$ of the phosphorus doped emitters can be observed and is in good correlation to other emitter studies [1,3,5,7].

4.2. Emitter saturation current density on untextured and textured surfaces for deep-diffused emitter profiles

The application of a surface texture generally increases the emitter saturation current density. For highly doped emitters the ratio between $J_{0e,textured}$ and $J_{0e,untextured}$ is in the range of 1.2–1.6. This corresponds quite well to an increase of the surface area, due to the inverted pyramids geometry, by a factor of about 1.7. However, for lightly doped emitters the ratio is well above the "geometry" factor. For an additional post-oxidation anneal time of 120 min, the factor even increased to a value of 3.9 (see Table II and Figure 8) due to the lower phosphorus doping concentrations at the surface and the deeper *p-n* junction. The emitter sheet resistance is decreased with the additional post-oxidation anneal.

This increase is explained by Glunz *et al.* [4] with the three-dimensional geometry of the inverted pyramids. The diffusion and thus the resulting emitter profiles on textured surfaces are not identical to the ones on untextured surfaces. In the top parts of the pyramids, an increased doping concentration may be present for a volume unit of silicon, whereas at the bottom, a lower concentration of doping atoms per silicon volume is available. On the side walls of the pyramids similar conditions as on untextured surfaces are expected. Due to the lower doping concentration at the bottom tips of the pyramids, the screening of recombination centers at the surface by lightly doped emitters is insufficient. This effect can also be deduced from the results of the emitter study performed by King *et al.* [1]

Table II. Ratio of the emitter saturation current density of untextured and textured surfaces determined in high and low injection regimes.

n+-diffusion (Ω/□)	$\rho_{base} = 0.5\,\Omega$ cm low injection regime	$\rho_{base} = 100\,\Omega$ cm high injection regime
	$J_{0e,text}/J_{0e,untext}$	$J_{0e,text}/J_{0e,untext}$
16	1.2	1.6
130	1.9	2.3
210	2.2	2.0
290	2.9	2.4
15[a]	1.4	1.2
220[a]	3.5	3.9

[a] Additional post-oxidation anneal time of 120 min.

Table I. Emitter saturation current density determined in high and low injection regimes at a temperature of 25°C for different diffused emitter profiles on untextured and textured surfaces.

	$\rho_{base} = 0{\cdot}5\,\Omega$ cm low injection regime				$\rho_{base} = 100\,\Omega$ cm high injection regime			
	untextured		textured		untextured		textured	
ρ_{sheet} (Ω/□)	J_{0e} (fA/cm^2)	$V_{oc,max}$ (mV)	J_{0e} (fA/cm^2)	$V_{oc,max}$ (mV)	J_{0e} (fA/cm^2)	$V_{oc,max}$ (mV)	J_{0e} (fA/cm^2)	$V_{oc,max}$ (mV)
16	172	675	206	660	144	679	225	658
130	16	736	30	710	14	739	33	708
210	10	748	22	718	10	748	20	721
290	8	754	23	717	9	751	23	717
15[a]	149	679	166	676	215	669	201	671
220[a]	11	746	38	714	11	746	43	710

[a] Additional post-oxidation anneal time of 120 min.

DOI: 10.1002/pip

4.3. Determination of emitter saturation current densities and surface recombination velocities on the basis of numerical simulations of effective carrier lifetimes

The emitter saturation current density can be determined experimentally for highly and lightly doped emitters for a wide range of substrate resistivities with the different methods in high and low injection regimes. Additionally, the effective minority carrier lifetimes which are determined by the IDLS can be simulated numerically with PC1D [20]. In PC1D the Fermi-Dirac distribution function is approximated by Boltzmann statistics, which is quite appropriate when the Fermi level is $> E_C$-3kT or $< E_V + 3$kT. Nevertheless, it is acceptable to perform the numerical device simulations with PC1D due to the fact that only lightly doped emitter profiles with $N_{P,0} < 10^{19}\,cm^{-3}$ are investigated. The simulations are based on a symmetrical structure with the same doping profiles on both sides. The applied phosphorus emitter profiles are shown in Figure 2. The substrate resistivities are 0.5 and 100 Ω cm. For the substrate resistivity of 0.5 Ω cm, the intrinsic bulk minority carrier lifetime of 706 µs, calculated by the Auger model of Kerr *et al.*, has been applied. A bulk minority carrier lifetime of 10 ms has been assumed for a substrate resistivity of 100 Ωcm. For the calculation of the average excess carrier density the spectrum of the flash lamp of the QSSPC measuring setup is used. The most important parameters for the numerical device simulations of the symmetrical test structures with PC1D are summarized in the appendix.

By varying the illumination intensity and calculating the average excess carrier density Δn_{av} and the cumulative photogeneration G of the symmetrical structure, the effective minority carrier lifetimes can be determined by $\tau_{eff} = \Delta n_{av}/G$, as already shown by Neuhaus *et al.* [21] The cumulative photogeneration has been additionally verified by ray tracing simulations with SUNRAYS [22], which employs Monte Carlo simulations and includes the exact geometry of the texture (inverted pyramids) and the material properties of the silicon oxide layer. The surface recombination velocity S_0 is then adjusted in PC1D in order to obtain a good agreement between simulated and measured carrier lifetime curves. The saturation current density of the emitter is calculated simultaneously corresponding to the determined S_0.

Figure 9 shows the measured and simulated effective carrier lifetime versus the excess carrier density for samples with untextured surfaces. The bulk minority carrier lifetime curves, including radiative recombination, Shockley–Read–Hall recombination and Auger recombination are also shown. For samples with a substrate resistivity of 100 Ω cm the simulations show that the bulk minority carrier lifetime is dominated by Shockley–Read–Hall recombination at low injections for the assumed bulk minority carrier lifetime of 10 ms and by Auger recombination at high injections. For both highly and lightly doped emitters, the effective carrier lifetime at high

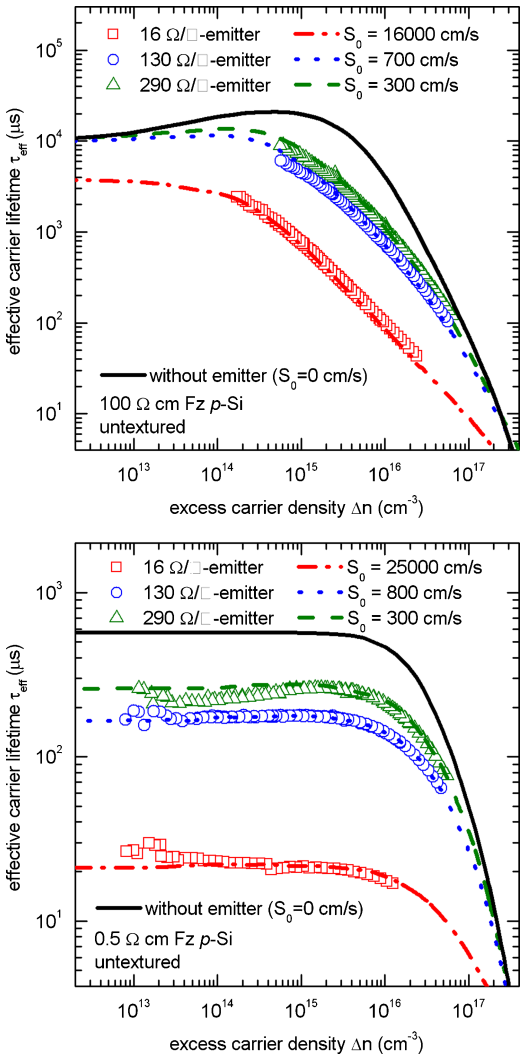

Figure 9. Effective carrier lifetime versus excess carrier density for untextured samples with different emitter profiles on *p*-type float-zone silicon with a substrate resistivity of 0·5 Ω cm (top) and 100 Ω cm (bottom). The lines represent the simulated values of the effective carrier lifetimes for different surface recombination velocities.

injections is limited by the emitter recombination. In contrast to lightly doped emitters, one can see that for highly doped emitters the effective carrier lifetime is limited by the emitter recombination over the entire injection range. The effective carrier lifetime of samples with a substrate resistivity of 0.5 Ω cm and different emitters are strongly affected by the Auger recombination at high injections. In low injection regimes, one can see that the Auger recombination (limited by the calculated intrinsic bulk minority carrier lifetime) is not the limiting factor in achieving high effective carrier lifetimes. In this case, the emitter recombination is dominant and reduces the effective carrier lifetimes by the constant amount of J_{0e}.

Table III. Emitter saturation current density determined under high and low injection regimes at a temperature of 25°C for different diffused emitter profiles on untextured and textured surfaces.

n+-diffusion (Ω/□)	$\rho_{base} = 0{\cdot}5\,\Omega\,cm$ low injection regime	$\rho_{base} = 100\,\Omega\,cm$ high injection regime	$\rho_{base} = 0{\cdot}5\,\Omega\,cm$ (simulations)	$\rho_{base} = 100\,\Omega\,cm$ (simulations)
	J_{0e} (fA/cm^2)			
	untextured			
16	172	144	143	91
130	16	14	14	13
210	10	10	12	11
290	8	9	9	10
15[a]	149	215	149	119
220[a]	11	11	13	12
	textured			
16	206	225	161	172
130	30	33	24	21
210	22	20	21	23
290	23	23	19	17
15[a]	166	201	167	187
220[a]	38	43	41	39

[a] Additional post-oxidation anneal time of 120 min.

A good agreement is obtained between the simulations of the surface recombination velocities for a substrate resistivity of 0.5 and 100 Ω cm. The corresponding values for J_{0e} are shown in Table III.

The presented way to determine the surface recombination velocity of highly and lowly doped emitters is the numerical simulation of effective carrier lifetimes with PC1D. Another way is the analytical calculation of S_0 as proposed by Cuevas *et al.* [3] A comparison of the surface recombination velocity versus the phosphorus doping concentration at the surface is shown in Figure 10 for both the numerical device simulations and the analytical approach. One can observe a good agreement between the numerically simulated and analytically calculated values. As already reported by various authors [1,3,5], S_0 decreases with a decreasing phosphorus doping concentration at the surface.

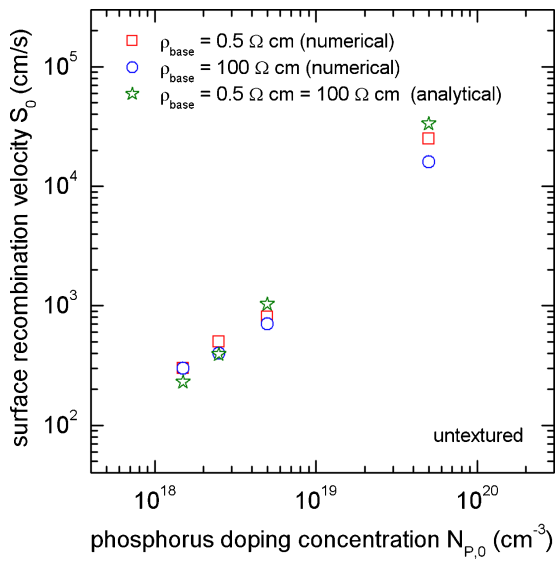

Figure 10. Surface recombination velocity versus phosphorus doping concentration simulated for *p*-type silicon with a substrate resistivity of 0·5 and 100 Ω cm.

A comparison of the determined emitter saturation current densities for the methods in high and low injection regimes and for the values of J_{0e}, calculated by numerical device simulations, is shown in Table III. A good agreement can be observed for the values of J_{0e} determined at high-level and low-level injection and by numerical device simulations.

5. SUMMARY AND CONCLUSIONS

In this study, the emitter saturation current density J_{0e} of differently doped phosphorus emitters was measured by means of IDLS in high and low injection regimes. The influence of various models for the Auger recombination on the evaluation of J_{0e} was investigated. For highly injected substrates, the model of Sinton *et al.*, Kerr *et al.*, and Glunz *et al.* can be applied when the excess carrier density is one order of magnitude higher than the substrate doping concentration. In this case, the different models for the Auger recombination result in the same values of J_{0e}. However, the model of Kerr *et al.* can be applied for much higher excess carrier densities. Due to the nonlinearity of the model of Schmidt *et al.* over a wide range of excess carrier densities, the extracted values for J_{0e} are not reliable. With the Auger parameterization of Kerr *et al.* the intrinsic bulk minority carrier lifetime at low injections can be calculated, giving an upper bound for J_{0e} and thus a

more conservative estimation. In this study the Auger parameterization of Kerr *et al.* is used because a wide range of excess carrier densities can be used to determine J_{0e} accurately in high and low injection regimes.

The results for samples with different phosphorus emitter doping profiles on textured and untextured surfaces show that J_{0e} decreases with decreasing surface doping concentration. However, on lightly doped emitters the surface texture has a detrimental impact on $J_{0e.}$ The investigations show that the values of J_{0e} are much higher than of the geometrical surface area ratio of 1.7 between textured and untextured surfaces.

Furthermore, numerical device simulations have been performed to determine the surface recombination velocity and the emitter saturation current density of the respective samples based on the measured effective carrier lifetime curves. A good correlation was found between the different methods at high and low injections and the numerical device simulation, showing that an accurate determination of J_{0e} is independent of the base resistivity and possible for both low and high resistivity substrates.

ACKNOWLEDGEMENTS

The authors gratefully acknowledge all members of the Department Silicon Solar Cells—Development and Characterization for their support and encouragement. Thomas Roth is recognized for fruitful discussions and Wesley Dopkins is acknowledged for carefully proofreading the manuscript.

APPENDIX

For the Auger recombination in heavily doped and/or highly injected silicon substrates, the Auger recombination coefficients are $C_n = 2.2 \times 10^{-31}\,\mathrm{cm}^6/\mathrm{s}$ for *n*-type and $C_p = 9.9 \times 10^{-32}\,\mathrm{cm}^6/\mathrm{s}$ for *p*-type silicon substrates. At high injections, the Coulomb-enhanced Auger recombination coefficient $C_A = 1.66 \times 10^{-30}\,\mathrm{cm}^6/\mathrm{s}$ is used [16]. The bandgap narrowing is calculated as proposed by Cuevas *et al.* with $A = 13.9\,\mathrm{meV}$ and $N_{ref} = 1.3 \times 10^{17}\,\mathrm{cm}^{-3}$ [3]. The mobility for holes is calculated by the maximum mobility coefficient of $470.5\,\mathrm{cm}^2/(\mathrm{Vs})$, and the minimum mobility coefficient of $155\,\mathrm{cm}^2/(\mathrm{Vs})$ with $N_{ref} = 1 \times 10^{17}\,\mathrm{cm}^{-3}$ and $\alpha = 0.9$ [3].

REFERENCES

1. King RR, Sinton RA, Swanson RM. Studies of diffused phosphorus emitters: saturation current, surface recombination velocity, and quantum efficiency. *IEEE Transaction on Electron Devices* 1990; **37**(2): 365–371.
2. King RR, Swanson RM. Studies of diffused boron emitters: saturation current, bandgap narrowing, and surface recombination velocity. *IEEE Transaction on Electron Devices* 1991; **38**(6): 1399–1409.
3. Cuevas A, Giroult-Matlakowski G, Basore PA, Dubois C. Extraction of surface recombination velocity of passivated phosphorus-doped silicon emitters. *IEEE First World Conference on Photovoltaic Energy Conversion*, Hawaii, USA, 1994; 1446–1449.
4. Glunz SW, Sterk S, Steeman R, Warta W, Knobloch J, Wettling W. Emitter dark saturation currents of high-efficiency solar cells with inverted pyramids. *Proceedings of the 13th European Photovoltaic Solar Energy Conference*, Nice, France, 1995; 409–412.
5. Cuevas A, Basore PA, Giroult-Matlakowski G, Dubois C. Surface recombination velocity of highly doped n-type silicon. *Journal of Applied Physics* 1996; **80**(6): 3370–3375.
6. Cuevas A, Stuckings M, Lau J, Petravic M. The recombination velocity of boron diffused silicon wafers. *Proceedings of the 14th European Photovoltaic Solar Energy Conference*, Barcelona, Spain, 1997; 2416–2419.
7. Kerr MJ, Schmidt J, Cuevas A, Bultman J. Surface recombination velocity of phosphorus-diffused silicon solar cell emitters passivated with plasma enhanced chemical vapour deposited silicon. *Journal of Applied Physics* 2001; **89**(7): 3821–3826.
8. Altermatt PP, Plagwitz H, Bock R, Schmidt J, Brendel R, Kerr MJ, Cuevas A. The surface recombination velocity at boron-doped emitters: comparison between various passivation techniques. *Proceedings of the 21st European Photovoltaic Solar Energy Conference*, Dresden, Germany, 2006; 647–650.
9. Sinton RA, Cuevas A, Stuckings M. Quasi-steady-state photoconductance, a new method for solar cell material and device characterization. *Proceedings of the 25th IEEE Photovoltaic Specialist Conference*, Washington D.C., USA, 1996; 457–460.
10. Kane DE, Swanson RM. Measurement of the emitter saturation current by a contactless photocunductivity decay method. *Proceedings of the 18th IEEE Photovoltaic Specialists Conference*, Las Vegas, USA, 1985; 578–581.
11. Cuevas A, Macdonald D. Measuring and interpreting the lifetime of silicon wafers. *Solar Energy* 2004; **76**: 255–262.
12. Cuevas A. The effect of emitter recombination on the effective lifetime of silicon wafers. *Solar Energy Materials & Solar Cells* 1999; **57**: 277–290.
13. Kerr MJ, Cuevas A. General parameterization of Auger recombination in crystalline silicon. *Journal of Applied Physics* 2002; **91**(4): 2473–2480.
14. Schmidt J, Kerr M, Altermatt PP. Coulomb-enhanced Auger recombination in crystalline silicon at intermediate and high injection densities. *Journal of Applied Physics* 2000; **88**(3): 1494–1497.
15. Glunz SW, Biro D, Rein S, Warta W. Field-effect passivation of the SiO_2-Si interface. *Journal of Applied Physics* 1999; **86**(1): 683–691.

16. Sinton RA, Swanson RM. Recombination in highly injected silicon. *IEEE Transaction on Electron Devices* 1987; **34**(6): 1380–1389.
17. Green MA. Intrinsic concentration, effective densities of states, and effective mass in silicon. *Journal of Applied Physics* 1990; **67**(6): 2944–2954.
18. Granek F, Reichel C, Hermle M, Huljić DM, Schultz O, Glunz SW. Front surface passivation of n-type high-efficiency back-junction silicon solar cells using front surface field. *Proceedings of the 22nd European Photovoltaic Solar Energy Conference*, Milano, Italy, 2007; 1262–1266.
19. Benick J, Leimenstoll A, Schultz O. Comprehensive studies of passivation quality on boron diffused silicon surfaces. *Proceedings of the 22nd European Photovoltaic Solar Energy Conference*, Milano, Italy, 2007; 1244–1247.
20. Clugston DA, Basore PA. PC1D version 5: 32-bit solar cell modeling on personal computers. *Proceedings of the 26th IEEE Photovoltaic Specialist Conference*, Anaheim, USA, 1997; 207–210.
21. Neuhaus DH, Cousins PJ, Aberle AG. Trapping and junction-related perturbations of the effective excess carrier lifetime. *Proceedings of the 3rd IEEE World Conference on Photovoltaic Energy Conversion*, Osaka, Japan, 2003; 91–94.
22. Brendel R. SUNRAYS: a versatile ray tracing program for the photovoltaic community. *Proceedings of the 12th European Photovoltaic Solar Energy Conference*, Amsterdam, The Netherlands, 1994; 1339–1342.